Journal Pre-proof

Influence of mixed plant protein combinations on the physicochemical, textural, structural and nutritional properties of extruded high-moisture meat analogues

Dayna Shu Min ONG, Xin Yi HUA, Alicia Hui Ping THENG, Bisma MUTIARGO, Hui Wen LEE, Raffael OSEN, Jie Hong CHIANG

PII: S0260-8774(25)00168-2

DOI: https://doi.org/10.1016/j.jfoodeng.2025.112633

Reference: JFOE 112633

To appear in: *Journal of Food Engineering*

Received Date: 30 October 2024

Revised Date: 7 April 2025

Accepted Date: 23 April 2025

Please cite this article as: Min ONG, D.S., Yi HUA, X., Ping THENG, A.H., MUTIARGO, B., Wen LEE, H., OSEN, R., Hong CHIANG, J., Influence of mixed plant protein combinations on the physicochemical, textural, structural and nutritional properties of extruded high-moisture meat analogues, *Journal of Food Engineering*, https://doi.org/10.1016/j.jfoodeng.2025.112633.

Influence of mixed plant protein combinations on the physicochemical, textural, structural and nutritional properties of extruded high-moisture meat analogues

Dayna Shu Min ONG [a], Xin Yi HUA [a], Alicia Hui Ping THENG [a], Bisma MUTIARGO [b], Hui Wen LEE [a], Raffael OSEN [a], Jie Hong CHIANG [a] *

[a] Singapore Institute of Food and Biotechnology Innovation (SIFBI), Agency for Science, Technology and Research (A*STAR), 31 Biopolis Way, Nanos, Singapore 138669, Singapore

[b] Intelligent Product Verification Group, Advanced Remanufacturing Technology Centre (ARTC), Agency for Science, Technology and Research (A*STAR), 3 Cleantech Loop, CleanTech Two, Singapore 637143, Singapore

*Contact information for the corresponding author:

Dr Jie Hong Chiang chiang_jie_hong@sifbi.a-star.edu.sg

Abstract

Plant proteins are known to contain lesser amounts of essential amino acids than animal proteins. This study explored using high-moisture extrusion to create six plant-based mixed protein matrices (MPM) at 50% and 60% moisture content to mimic the amino acid profile of chicken breast meat. X-ray computed tomography and textural analysis were employed to evaluate the structural and textural properties of these extruded MPM. Results revealed that extruded MPM containing 50% rice protein exhibited the highest hardness. Extruded MPM formulated with soy and pea proteins demonstrated the highest degree of texturisation at 55% moisture content, and soy and chickpea proteins at 60%. Chemical bond elucidation and Fourier-transform infrared spectroscopy revealed hydrogen bonds and β-sheets as the dominant forces stabilising the protein structure across all extruded MPM, regardless of the specific plant protein source. Additionally, the purine content of extruded MPM was lower compared to existing commercial vegetarian products. These findings underscore the potential of MPM derived from various plant protein combinations to produce meat analogues with a range of structural and textural attributes. This approach presents promising opportunities for tailoring MPM to meet the diverse preferences of consumers.

Keywords:

High-moisture meat analogues, mixed plant proteins, extrusion, imaging, texture, chemical bonds, purines

Abbreviations: MPM; mixed protein matrices, XCT; x-ray computed tomography, MC; moisture content, DT; degree of texturisation

1. Introduction

The increasing concern for environmental sustainability and personal health is driving a significant shift towards plant-based diets (Kołodziejczak et al., 2022). However, many consumers hesitate to completely replace meat due to perceived shortcomings in plant-based alternatives. These concerns often include imbalanced amino acid profiles and taste and texture discrepancies (Schmid et al., 2022). Therefore, it is crucial to develop plant-based meat analogues that closely resemble their animal meat counterparts in terms of taste, texture, and nutritional value to promote a reduction in meat consumption.

Extrusion processing has been the primary method for plant-based meat production since the 1960s, with proteins and starches forming the core ingredients (Osen et al., 2014). Traditionally, extruded plant-based meat analogues are categorised based on their water contents: low (10–40%) and high (40–70%) moisture. However, recent research has focused on commercialising high moisture extrusion (HME) due to its ability to create textures more akin to meat (Schmid et al., 2022). During HME, the product is forced through a cooling die, facilitating the formation of fibres that contribute to a meat-like texture. Several factors influence this texture development, including the protein source and the interactions between proteins and other ingredients within the formulation (Chen et al., 2017).

Soy protein has been the dominant choice in plant-based meat production due to its nutritional value and functional properties. Soy protein has also been used to enhance cereal-based foods due to its well-balanced amino acid profile compared to most other plant proteins (Li et al., 2005). However, soy, as well as other plant proteins, generally have a lower nutritional quality than meat proteins due to limitations in specific essential amino acids,

particularly methionine and lysine (van Vliet et al., 2015; Gorissen et al., 2018). While studies have identified combinations of different protein sources to achieve a balanced amino acid profile of plant-based foods (Woolf et al., 2011; Dimina et al., 2022), their impact on the texture and structural attributes of plant-based meats remains unexplored. This gap highlights the need for further research to fully understand how these protein matrices can be optimised to enhance overall product quality (e.g., texture). Beyond the nutritional shortcomings of single protein sources, their specific techno-functional properties may impose challenges for structuring. For example, the structuring of pea protein can be challenging due to its weaker gelling capacity and heat-induced gelation than that of soy protein isolates (Schreuders et al., 2019). On the other hand, some soy-based meat analogues have been reported to contain elevated levels of dietary purines, potentially posing health risks for individuals with hyperuricemia (Havlik et al., 2010).

In our previous study, Hua et al. (2023) reported the use of mathematical optimisation on the blending of various protein ingredients, including wheat gluten, chickpea, pea, mung bean, and rice. Six formulations of mixed protein matrices (MPM) were obtained, which were designed to mimic the amino acid profile of chicken breast meat. In this continuation study, the limitations in current plant-based meat analogues are addressed by developing MPM with enhanced amino acid profiles. The structural, textural, chemical and nutritional properties of these extruded MPM were comprehensively evaluated.

2. Materials and methods

2.1 Materials

High-moisture mixed protein matrices (MPM) produced from the previous study by Hua et al. (2023) used various plant proteins from multiple commercial sources. These included Wilmar International Ltd (WILCON; soy protein concentrate – brand 1) and Connell Caldic Malaysia Sdn Bhd (ALPHA® 8; soy protein concentrate – brand 2), which, as detailed in (Hua et al., 2023), exhibited differences in their protein contents and amino acid profiles. The study also incorporated pea protein isolate (NUTRALYS® F85M; Roquette Singapore), chickpea protein concentrate (B 75%; Nutraonly Nutrition Inc., China), mung bean protein isolate (Munptein™; ETprotein, China), wheat gluten (BeneoPro VWG 75) and rice protein isolate (RemyPro N85) (Beneo Asia-Pacific Pte Ltd.). The comprehensive protein and amino acid profiles of all these ingredients, including variations between the two SPCs, have been reported previously (Hua et al., 2023). Bovine serum albumin (BSA) powder, potassium dihydrogen orthophosphate, di-potassium hydrogen orthophosphate, sodium dodecyl sulphate (SDS), 1,4-dithiothreitol (DTT), urea, and Bradford reagent were bought from Sigma-Aldrich, Singapore. Formaldehyde and glutaraldehyde were purchased from Electron Microscopy Science, USA. Adenine, guanine, hypoxanthine, uric acid, xanthine, hypoxathine-$^{13}C_2$,^{15}N, uric acid-^{13}C,$^{15}N_3$, xanthine-^{13}C,$^{15}N_2$ standards were purchased from Axil Scientific Pte Ltd (Singapore). Ultrapure water was purified using Milli-Q equipment (Millipore Corporation, Massachusetts, USA). All other reagents and chemicals used were of analytical grade.

2.2 High-moisture extrusion

A laboratory, co-rotating and intermeshing twin screw extruder (Process 16 Hygienic, Thermo Fisher Scientific, Germany) with a screw diameter of 16 mm, a smooth barrel and a length-diameter ratio of 40:1 was used for the extrusion experiments. The formulations of MPM employed in this study were derived from the mathematical optimisation process described by Hua et al. (2023). **Table 1** presents the specific combinations of plant proteins used in each formulation. The extrusion screw profile comprised of (from feed to exit): fifteen 16 mm feed screws (240 mm); twelve 4 mm mixing elements (48 mm); eight 16 mm feed screws (128 mm); ten 4 mm mixing elements (40 mm); ten 16 mm forward screws (160 mm); and one 24 mm discharge element (24 mm). The barrel was segmented into the feeding zone, and seven temperature-controlled zones heated by an electric cartridge system and cooled with water. A long die with dimensions of 83 × 49 × 188 mm ($W \times H \times L$) and an opening of 28 × 6 mm ($W \times H$) was used. Water at 80°C as a cooling medium was attached at the end of the extruder. Dry materials were fed into the extruder using a gravimetric feeder (Brabender Technology GmbH, Duisburg, Germany) at a feed rate of 1.8 kg/h. Simultaneously, a 1% (w/w) salt solution was injected via a peristaltic pump (Masterflex L/S, Vernon Hills, USA) into the second barrel at different flow rates for various formulations. This aimed to achieve a final moisture content (MC) of approximately 55% or 60% (wet basis) in the MPM. The screw speed was maintained at 400 rpm, and the barrel temperature profile was set at 40, 60, 80, 100, 120, 120, 140, and 140°C in the eight zones from feed to die. The extruded MPM were named using a format of "formulation-moisture content" (e.g., F1-55 indicates the sample containing formulation F1 from **Table 1** with MC of 55% w/w). Sample F6-60 was not collected due to extrusion difficulties (i.e., flashing) likely caused by the high MC that potentially affected the flow behaviour inside the extruder.

[Insert **Table 1**]

2.3 Physicochemical analysis

Protein content: The protein content of extruded MPM was determined using an automated Dumas protein analyser (Dumatherm® N Pro, Gerhardt GmbH, Germany). For each analysis, 100 mg of samples were used, and a nitrogen conversion factor of 5.7 for wheat gluten and 6.25 for all other plant proteins (Jones, 1931).

Moisture content: Moisture content was determined in an air oven. Numbered pans and lids were weighed prior to the analysis, and 2 g of samples were weighed into the pans. The samples were then placed into an oven (111 Eco Linem Venticell, Germany) at 105 °C for 24 h and cooled in a desiccator for an hour after. Subsequently, the weight of the samples was recorded.

2.4 X-ray computed tomography (XCT)

The samples were prepared according to Nieuwland et al. (2023) for visualisation using X-ray computed tomography. However, due to the suboptimal freezing conditions required to keep the sample frozen during the scanning, the samples were partially thawed, hindering the observation of lamella. To overcome this, the samples were chemically fixed instead of just freeze-drying (Zhao & Takhar, 2017) to remove water without altering their structure, enabling clear visualisation of density differences. Chemical fixation was carried out in a solution containing 0.1 M phosphate buffer (pH 7.2) with 2% formaldehyde and 3%

glutaraldehyde (electron microscopy grade) for at least 8 hours, as described by Chiang et al. (2019). After fixation, samples were dehydrated through a graded series of ethanol solutions, up to 100% ethanol, to remove water. Subsequently, the samples were frozen and freeze-dried at -80°C and 0.01 mbar for 72 hours.

The dried samples were then visualised with X-ray computed tomography according to Tham et al. (2024) with modifications. Samples were mounted onto a carbon fibre fixture and scanned using a computed tomography scanner (X TH 225 st, Nikon, Japan) as shown in **Supplementary Materials – Figure S1**. The scan parameters were set at 170 kV beam energy, 15 W of power (corresponding to an approximate spot size of 0.015 mm), and no beam hardening filter was used. Each image was captured twice to reduce noise with a low exposure of 0.7 sec and a high detector gain of 24 dB. A total of 1000 frames were captured over a full 360° of rotation. The data was reconstructed using CTPro software (version 1.1.1-b). The voxel size achieved in this scan was a high resolution of 0.04 mm. Following reconstruction, slices were manually aligned using VGStudio (version 2023.4, Volume Graphics, Germany). Three-centred representative reconstructed slices (longitudinal view) were chosen for further analysis using ImageJ (version 1.54h, National Institutes of Health, U.S). The images were subjected to thresholding to distinguish pores (dark) from the material (light). The image was then inverted, and a particle filter was applied to exclude features smaller than 300 pixels, likely representing background noise (**Figure 1**). This process allowed the isolation of pores to calculate the total pore percentage.

[Insert **Figure 1**]

2.5 Textural analysis

2.5.1 Textural Profile Analysis (TPA)

The textural properties of the samples were determined using a textural analyser (TA.XT Plus, Stable Micro Systems, UK) with a two-bite test method adapted from Chiang et al. (2019). Samples (15 × 15 mm, length × width) were subjected to compression with a P/75 probe at a speed of 1 mm/s. The first bite compressed the sample to 50% of its original thickness, followed by a 5-sec relaxation period where the probe returned to its starting position. The second bite then compressed the sample again to 50% of the thickness achieved in the first compression. Hardness and chewiness were measured from the resulting force-displacement curves generated during this two-bite test.

2.5.2 Cutting force

A cutting test was performed to assess the fibrous structure formation within the samples (Chiang et al., 2019). Each sample (15 × 15 mm, length × width) was cut using a craft knife adapter (A/CKB) at a speed of 1 mm/s. The cutting depth was set to 75% of the original sample thickness. This analysis evaluated the force required to cut through the samples in two directions: longitudinal/ lengthwise (parallel to the outflow direction of the extruder) and transverse/ crosswise (perpendicular to the outflow direction of the extruder).

2.6 Protein solubility analysis

Protein solubility was assessed to understand the influence of different chemical bonds on protein interactions within the samples. The method employed was adapted from Wang et al. (2018). Four extraction solutions were prepared to target specific bonds: (1) P (PB; 0.1 M

phosphate buffer consisting of KH_2PO_4 and K_2HPO_4 with a pH of 7.5, native state protein), (2) PU (PB + 8 M Urea; hydrogen bonds), (3) PD (PB + 0.05 M DTT; disulphide bonds), and (4) PS (1.5 g/100 ml SDS, hydrophobic interactions).

For each sample, 0.5 g was treated with 10 ml of an extraction solution. The mixture was agitated on a shaker (LSE™, Corning, Slovenia) at 400 rpm for 30 min. This was followed by high shear homogenisation at 12,000 rpm for 30 sec to disrupt protein-protein interactions further. After another 30-min agitation, the suspension was centrifuged at 2580×*g* for 10 min at 25°C. The supernatant, containing solubilised proteins, was transferred to an Eppendorf tube and centrifuged again at a higher speed (9300×*g* for 10 min at 25°C) to remove any remaining insoluble material. Protein concentration in the resulting supernatants was determined using a Bradford assay performed on a cell imaging multi-mode reader (Cytation 5, BioTek, USA) at 595 nm. Briefly, 5 µl of the supernatant was mixed with 250 µl Bradford reagent in a 96-well plate. BSA powder served as the standard for the assay. Protein solubility was calculated as the percentage of protein solubilised by the specific extraction solution compared to the total protein content in the original sample.

2.7 Secondary structures

The secondary structure of the samples was determined using Fourier transform infrared spectroscopy (Nicolet iS50, Thermo Fisher Scientific, USA) with attenuated total reflectance sampling (ATR-FTIR) according to the method described by Wang et al. (2022c). Extrudates were sliced into a thickness of 2 mm and placed onto the diamond surface of the ATR cell before each scan. Samples were scanned 64 times at a resolution of 4 cm^{-1} across a

223 wavenumber range of 4000 – 500 cm^{-1}. The infrared spectrum of the protein secondary
224 structures was captured within the amide I band (1700 – 1600 cm^{-1}) using the OMNIC
225 software (Nicolet Co., USA). Following data acquisition, Gaussian deconvolution was applied
226 to separate overlapping peaks within the amide I band. Water was used as a baseline before
227 measuring all samples, and was subtracted from the sample spectrum to correct for any
228 interference caused by water. The relative proportions of each secondary structure were then
229 determined based on the integrated area of the corresponding subpeaks.
230

231 2.8 Purine analysis

232 Purine analysis was performed for selected extruded MPM with 55% MC to quantify adenine,
233 guanine, hypoxanthine, uric acid, and xanthine levels. To ensure homogeneity, samples were
234 blended with ultrapure water at a 1:2 w/w ratio using a high-speed shearer (12,000 rpm, 1
235 min) to create a slurry. From the slurry, 100 mg was mixed with 2 ml of 3 M sulphuric acid and
236 incubated at 100°C for 1 hour to extract the purines. The extract was then neutralised with 2
237 ml of 6 M sodium hydroxide. Before sample injection, the neutralised extracts were diluted
238 20-fold for adenine and guanine analysis and 2-fold for hypoxanthine, uric acid, and xanthine
239 analysis. The concentration of internal standards (hypoxathine-$^{13}C_2$,^{15}N, uric acid-^{13}C,$^{15}N_3$,
240 xanthine-^{13}C,$^{15}N_2$) was 50 ng/ml after dilution. Individual purine stock solutions were
241 prepared in water (for adenine, hypoxanthine and hypoxathine-$^{13}C_2$,^{15}N) or 10% v/v of 0.1 M
242 sodium hydroxide (for guanine, xanthine, uric acid, and corresponding internal standards),
243 and working standards were prepared from dilutions of stocks with 0.1% v/v formic acid.
244

245 A Shimadzu Prominence LC-20AD system (Kyoto, Japan) coupled with a Shimadzu triple
246 quadrupole mass spectrometer (LCMS-8050) equipped with an electrospray ionisation (ESI)

source was used to analyse purine content. The autosampler (SIL-30AC) and column oven (CTO-20A) were maintained at 4°C and 30°C, respectively. The purines were separated by mobile phases consisting of 0.1% v/v formic acid (solvent A) and 50% v/v methanol (solvent B) delivered at 0.4 ml/min. The gradient elution programme was as follows: 2% B (0–2 min), 15% B (2–3 min), 15–50% B (3–10 min), 50–98% B (10–10.1 min), 98% B (10.1–13 min), 98–2% B (13–13.1 min), and 2% B (13.1–17 min). The ESI source parameters were: nebulising gas flow of 2.5 L/min, heating gas flow of 20 L/min, interface temperature of 350°C, desolvation temperature of 150°C, and heat block temperature of 400°C. Purines were detected in multiple reaction monitoring (MRM) modes using optimised transitions established through flow injection analysis of individual standards and referencing literature (Lendoiro et al., 2012; Ge et al., 2016; Monostori et al., 2019; Muguruma et al., 2020).

2.9 Data analysis

All measurements were performed in triplicate, and results are reported as mean values ± standard deviation (SD). Statistical analysis was performed using Minitab 17 software (Minitab Inc., USA). One-way analysis of variance (ANOVA) with Tukey's post-hoc test for pairwise comparisons ($p \leq 0.05$) was used to assess significant differences between samples. Data visualisation was performed using Origin 2020 software (OriginLab Corp, USA).

3. Results and discussion

3.1 Physicochemical properties

The protein and moisture content of extruded MPM at 55% MC and 60% MC were present in **Table 2**. An increase in moisture content led to reduced protein content due to the higher

amount of water being fed into the extruder, diluting the protein content (with a fixed feed rate of 1.8 kg/h). F4 and F6 exhibited the highest protein contents, potentially attributed to the higher amount of protein ingredients used, which typically have protein contents exceeding 80% (**Supplementary Materials – Table S1**). The results also indicated that with the exception of F1-60, the extruded MPM showed higher protein content compared to the cooked chicken breast (28.94 ± 0.25%), as reported by Chiang et al. (2021). Conversely, the moisture content of the extruded MPM was lower than that of cooked chicken breast (71.46 ± 0.32%).

The measured moisture content of extruded MPM at 55% MC and 60% MC varied, which aligned with the finding of Zahari et al. (2020), who observed a similar discrepancy between target and actual moisture content in meat analogues. Varying water feed flow rates (i.e., 1.92 to 2.55 kg/h) during extrusion were likely responsible for this deviation. Different protein combinations with varying water-holding capacity (WHC) can also impact the overall moisture content of extruded MPM (Godschalk-Broers et al., 2022).

[Insert **Table 2**]

3.2 Macrostructure

3.2.1 Cross-sectional view

The colourimetric (L*a*b*) values for the exterior surface of extruded MPM at 55% MC were reported in our previous study (Hua et al., 2023). **Figure 2** visually depicts the internal structure of the extruded MPM at different MCs. Cross-sectional views revealed that all formulations, except for F2 (differentiated by CPC), exhibited a more prominent fibrous

structure at 55% MC compared to 60% MC. We hypothesised that in F2 at 55% MC, hydrophobic proteins limited chickpea starch gelatinisation and hindered fibre formation, whereas 60% MC improved gelatinisation and fibre development (Scott & Awika, 2023). These fibrous structures, however, consisted of thinner strands than those observed in cooked chicken breast (Chiang et al., 2021). This observation aligns with previous research by Zhang et al. (2020), who reported a decrease in anisotropy in pea protein extrudates with increasing MC. In a study by Guo et al. (2020), it was also found that an increase in MC from 60% to 90% resulted in the disappearance of layered structures in meat analogues made with soy protein and wheat gluten. This was due to the increased fluidity of the material, which lowered the shear strength and pressure exerted onto the material.

The type of protein used plays a role in fibre formation within the extruded MPM. A study by Schreuders et al. (2019) compared texturised PPI-WG and SPI-WG blends using a high-temperature conical shear cell. The findings showed that PPI-WG produced weak gels with small fibres at 110°C, while SPI-WG exhibited fibrous morphology across all temperatures. This indicates that PPI-WG blends produced meat analogues with smaller and thinner fibres. This aligns with the observations in **Figure 2**, where extruded MPM containing PPI and WG (F5 and F6) displayed thin, well-defined fibres as compared to the other formulations. Conversely, MPM containing SPC and WG (F1 and F2) exhibited thick fibres that were densely packed together.

[Insert **Figure 2**]

317 3.2.2 Porosity

318 During extrusion, air bubbles play a pivotal role in the formation of fibrous structures and
319 anisotropic properties (Taghian Dinani et al., 2023). While visual assessment is a common
320 practice, its subjective and qualitative nature can limit its effectiveness (Ranasinghesagara et
321 al., 2005). To address this, X-ray computed tomography (XCT) was conducted to provide
322 quantitative information regarding the internal structure of extruded MPM, including the
323 porosity. Although fibrous networks were observed on the fresh extruded MPM, the XCT scan
324 revealed a homogenous density distribution in the partially thawed sample (image not
325 shown), similar to findings by Nieuwland et al. (2023). In XCT images on samples which were
326 chemically fixated (**Figure 2**), darker regions represent areas with lower density (pores), while
327 brighter regions indicate areas with higher density (protein-rich regions). The freeze-drying
328 process following chemical fixation removes water, transforming water-rich regions into air
329 pockets, as confirmed by the presence of pores (Wittek et al., 2021).

330

331 Analysis of the morphology revealed that most extruded MPM exhibited anisotropic or
332 lamella structures, particularly those processed at 55% MC (**Figure 2**). During extrusion, the
333 temperature gradient within the cooling channel resulted in the preferential solidification of
334 the melt mixture near the cooled metallic surface, which in turn created a viscosity gradient
335 within the extrudate. As a result, Hagen-Poiseuille flow, characterised by a parabolic velocity
336 profile, was observed along the extrusion direction (**Figure 2**). This flow pattern contributed
337 to the formation of the anisotropic V-shaped structures observed in the extrudates (Lee et al.,
338 2023). The different plant protein combinations resulted in distinct morphologies, as shown
339 in **Figure 2**. In multiphase systems, proteins exhibit varying degrees of hydrophilicity (Wittek
340 et al., 2021). This variation directly influences the water distribution and rheological

properties of individual phases within the MPM, ultimately leading to differences in the development of the final morphology. However, due to the complexity of the XCT images, quantifying the wedge length and lamella thickness was not feasible. Instead, porosity analysis was conducted to assess the structural properties of the MPM. It was hypothesised that pore development occurred at the cooling die exit due to the release of pressure upon exit, enabling the growth of steam bubbles from the high melt temperatures (170 to 185°C) (van der Sman & van der Goot, 2023).

XCT images revealed that MC significantly influenced the porosity of extruded MPM (**Table 2**). Increasing MC from 55% to 60% resulted in a decrease in porosity for F2, F3, and F5. This observation aligns with the visual assessment of XCT images (**Figure 2**), where MPM at 60% MC displayed fewer dark areas indicating pores. However, F1 and F4 exhibited contrasting trends. While F1 showed no significant change in porosity, F4 displayed an increase in porosity with increased MC. This difference was attributed to the varying water-holding capacities of the protein ingredients used (Lee et al., 2022b). RPI, the major source of protein in F4 (at 50%), had the second lowest WAC (1.78 g water/ g protein) amongst all other proteins. This translates to a lower ability of F4 to bind water during extrusion, resulting in a higher amount of free water within the extrudate structure, exhibiting larger air pockets and higher porosity (**Figure 2**). When the MC of F4 increased further from 55% to 60%, more free water was present within the extrudate structure, leading to an increase in porosity observed in **Table 2**.

The XCT images did not fully capture the visually observed fibres in F1 and F5 at both MC levels, and in F3-60 (**Figure 2**). This observation aligns with findings by De Angelis et al. (2023),

365 who showed that visually evident fibres in meat analogues extruded at 125 and 145°C at 40%
366 MC were not adequately visualised using XCT. During extrusion, high temperatures and water
367 evaporation contribute to the formation of air pockets within the material, impacting the final
368 product properties (Dekkers et al., 2018). As XCT relies on differences in material densities for
369 image generation, it may struggle to distinguish between components with similar densities,
370 such as the protein biopolymers in the extruded MPM (Schreuders et al., 2021). The air
371 pockets, possessing notably different densities compared to the protein material, were
372 readily detected by XCT (**Figure 2**). Conversely, the protein biopolymers, with densities similar
373 to the surrounding matrix, remained indistinguishable, leading to the absence of
374 anisotropicity in the XCT images. This phenomenon aligns with the observations reported by
375 Schreuders et al. (2021) for SPI and pectin gels.
376

377 ## 3.3 Texture properties

378 3.3.1 Hardness

379 The textural properties of extruded MPM, including hardness, chewiness, and springiness,
380 were evaluated (**Table 2**). Due to the absence of significant differences (p=0.147), the
381 springiness results for the extruded MPM are not shown. Since all samples were processed
382 under identical extrusion parameters besides MC, the observed variations in hardness and
383 chewiness can be primarily attributed to the different plant protein compositions of the MPM
384 formulations.
385

386 Given the positive correlation between hardness and chewiness (a function of hardness)
387 (Mateen & Singh, 2023), the chewiness results were not discussed in detail. The hardness of
388 the extruded MPM decreased as MC increased from 55% to 60% (**Table 2**). Increasing the

389 water content in the extruder reduced die pressure, leading to fewer cross-linking reactions
390 between protein molecules (Snel et al., 2024). This resulted in incomplete protein
391 texturisation (Lin et al., 2000). Additionally, protein molecules require the exposure and
392 alignment of reactive sites for new intermolecular linkages to form (Schmid et al., 2022).
393 Increasing MC reduced protein concentration in the mixture, lowering the number of
394 potential reactive sites for cross-linking. Hence, the extruded MPM at 60% MC were softer
395 than those at 55% MC. These findings align with previous research suggesting that an increase
396 in MC can disrupt the formation of rigid protein networks, resulting in softer-textured
397 extrudates (Ferawati et al., 2021). However, despite the decrease in hardness with increased
398 MC, the hardness of extruded MPM remained considerably higher than that of cooked
399 chicken breast (40.53 – 55.01 N), which was reported by Chiang et al. (2019) and Chiang et al.
400 (2021). The harder texture of extruded MPM compared to cooked chicken breast could be
401 likely attributed to protein denaturation and aggregation caused by the high temperatures
402 and intense shear forces experienced during extrusion. The extrusion process leads to a more
403 structured and interconnected protein network, which contributes to the increased hardness.
404
405 When comparing extruded MPM within the same MC, F4, containing a higher proportion of
406 RPI, exhibited the highest hardness (**Table 2**). This might be attributed to the lower water
407 absorption capacity (WAC) of RPI compared to SPC (Zhao et al., 2020), which is also shown in
408 **Supplementary Material - Table S2**. The low WAC was due to the presence of water-insoluble
409 glutelin in RPI, which is crucial for water interaction (Lee et al., 2022b). While WAC is a
410 complex property influenced by various factors, direct comparisons between plant protein
411 sources can be challenging due to the variations in units used by different researchers (Jarpa-

412 Parra, 2018). The precise mechanism by which native protein WAC impacts the properties of
413 textured proteins remains an area of ongoing investigation (Webb et al., 2023).
414
415 In addition, the gelling properties of protein sources can influence the texture properties of
416 extruded MPM. Proteins with higher minimum gelation concentrations exhibit poorer gelling
417 properties. Lower viscosity, shorter residence times in the extruder barrel, and reduced
418 mechanical and thermal energy input can all contribute to this, limiting the formation of
419 strong protein networks (Lee et al., 2022a). F5-60, with a higher proportion of PPI, displayed
420 one of the lowest hardness compared to other extruded MPM (**Table 2**). This aligns with the
421 known limited gelling capacity of PPI, which forms weaker and less elastic gels than SPI (Shand
422 et al., 2007). The selection of raw materials, as exemplified by the higher PPI content in F5
423 and F6, can significantly impact the textural properties of the extruded MPM.
424
425 3.3.2 Degree of texturisation
426 The degree of texturisation (DT) reflects the anisotropy of the extruded MPM, with higher
427 values indicating a more pronounced longitudinal fibrous structure resembling animal muscle
428 fibres (Lee et al., 2023). DT is calculated as the ratio of transverse cutting strength to
429 longitudinal cutting strength. Values lower or close to 1 suggest a weak or absent fibrous
430 texture (Osen et al., 2014). As mentioned by van der Sman and van der Goot (2023), the
431 lamella structures of extrudates may be influenced by an interaction between a syneresis
432 process and the presence of a second biopolymer phase. In this study, two or more protein
433 sources were used, which indicates that such interactions may be present during the
434 structuring process of the MPM. This is also shown in the results in **Table 2**, whereby all

435 extruded MPM exhibited DT values greater than 1, indicating the presence of well-developed
436 fibrous structures.
437
438 MC influences the interaction between protein and water molecules during extrusion. This
439 would alter the microstructure, water distribution, and secondary structures within the
440 extrudates (Xia et al., 2023). Generally, a decrease in DT is observed with an increase in MC
441 from 55 to 60% (**Table 2**). However, F2 displayed a reduction in hardness and chewiness but
442 an increased DT with increasing MC instead. This observation could be attributed to the
443 presence of chickpea protein (CPC), which is the primary protein source in F2, and was absent
444 in other formulations. Wang et al. (2022a) highlighted that the textural properties of
445 extrudates are influenced by the composition of starch and proteins in the ingredients. As the
446 CPC used in this study contained ~13% starches based on the manufacturer's specification
447 (**Supplementary Material – Table S1**), it could have explained the observed trends in the
448 textural properties of F2.
449
450 F5-55 had the highest DT (**Table 2**), seemingly contradicting the absence of fibres in the
451 corresponding XCT image (**Figure 2**). As discussed earlier, the limitation of XCT in
452 distinguishing protein biopolymers with similar densities to the matrix likely explains this
453 discrepancy. While XCT may not have captured the fibres, the high DT of F5-55 aligns well
454 with the presence of thin, well-defined fibres observed visually in **Figure 2**. This suggests that
455 these fibres, although not visualised by XCT, contributed substantially to the high DT.
456 Furthermore, all DT values in this study were above 1, indicating a texturised structure for all
457 extruded MPM. This aligns with the visual observation in **Figure 2**, where all extruded MPM
458 display fibrous structures. This suggests that the XCT images were only accurate in predicting

459 the amount of air bubbles (i.e., porosity) present within extruded MPM, but not in capturing
460 the fibrous networks.
461

462 3.4 Chemical bond elucidation by selective solubilisation

463 Protein solubility analysis was performed to elucidate different classes of intermolecular
464 bonds (i.e., disulphide bonds, hydrogen bonds, and hydrophobic interactions) present within
465 the extruded MPM at 55% MC. Phosphate buffer (PB), known to disrupt proteins in their
466 native state (Liu & Hsieh, 2008), extracted the lowest amount of protein from all extruded
467 MPM. This phenomenon is attributed to the denaturation and aggregation of proteins during
468 the high-temperature and high-shear environment of the extrusion process (Chiang et al.,
469 2019). When DTT, urea, or SDS were mixed with PB, the amount of protein extracted from
470 the extruded MPM increased. This indicated the presence of more than one type of chemical
471 bond within the aggregated proteins in extruded MPM. Similar to the findings reported by
472 Chiang et al. (2021), the highest protein extraction was achieved using PU, suggesting a
473 predominance of hydrogen bonds. Disulphide bonds and hydrophobic interactions,
474 associated with PD and PS, respectively, followed in protein extraction efficiency, indicating
475 their relatively lower impact on the aggregated protein structure. Given the overlapping
476 solubilisation properties of the extraction solutions and the potential for redundancy in
477 information, the analyses involving more than two buffers were not conducted, as they may
478 not provide significant additional insights.
479

480 [Insert **Figure 3**]
481

As highlighted by Chiang et al. (2019) and Zhang et al. (2022), disulphide bonds are the primary force driving the formation of fibrous structures in extruded meat analogues. The amount of protein extracted by PD closely correlated with the DT of extruded MPM **(Table 2**), except for F5-55. F6-55 exhibited the lowest DT and, correspondingly, the lowest level of protein solubility in PD (**Figure 3**), suggesting a lower content of disulphide bonds. This aligns with Chiang et al. (2019), who observed that extrusion of SPC/WG composites with lower amounts of WG resulted in reduced disulphide linkages, lower DT, and poorer fibrous structure. Given that SPC contains fewer sulphur-containing amino acids (AA) compared to WG (Mariotti, 2017), it was evident that a lower content of these AA resulted in reduced fibre formation. The presence of MBPI, known to be deficient in sulphur-containing AA (Brishti et al., 2021), likely contributed to the lower DT and protein solubility in F6-55 (**Supplementary Materials – Table S3**).

Non-covalent interactions like hydrogen bonds and hydrophobic interactions are often reported to play a more significant role than disulphide bonds in stabilising the rigid protein structures of meat analogues (Osen et al., 2015; Chiang et al., 2019). F5-55 displayed the highest PU solubility among the extruded MPM (**Figure 3**). This suggests a higher hydrogen bond content compared to other formulations and aligns with the finding that PPI exhibited higher extractable PU proteins than SPI (Wang et al., 2022b). This could also explain the greater protein solubility in PU for F5-55 compared to F1-55 (**Figure 3**), which contained 92% SPC and no PPI.

3.5 Secondary structures

FTIR analysis was performed on extruded MPM at 55% MC to investigate their secondary structures, where the spectra are shown in **Supplementary Materials – Figure S2**. The amide I region (1600-1700 cm^{-1}), corresponding to C=O stretching vibrations, was analysed to identify functional and structural groups associated with protein secondary structures (**Table 3**). This region typically reveals peaks associated with β-sheets (1615-1637 cm^{-1}), random coils (1637-1645 cm^{-1}), α-helices (1646-1664 cm^{-1}), and β-turns (1664-1681 cm^{-1}) (Peng et al., 2021). No significant differences in the wavenumber positions of the absorption bands were observed among the extruded MPM across any of the protein secondary structure bands (data not shown). This suggests that the extrusion conditions used in this study did not significantly alter the overall secondary structure profile of the proteins.

[Insert **Table 3**]

FTIR analysis of extruded MPM revealed insights into their secondary structures (**Table 3**). Extruded MPM generally exhibited a similar trend, with β-sheets being the most prevalent conformation, followed by random coils, α-helices, and β-turns. Notably, β-sheet and random coil structures together constituted over 70% of the total secondary structures, indicating their dominance in the protein network. Extrusion is known to promote the conversion of α-helix structures to β-sheets in plant proteins (Wang et al., 2024). This phenomenon likely contributed to the high prevalence of β-sheets observed in extruded MPM.

β-sheet structures typically form when proteins unfold and aggregate, resulting in a more rigid and less flexible structure (Guo et al., 2020; Peng et al., 2022). Random coil represents a loose and disordered region of a protein where it results from the disruption of secondary structures (β-sheet and α-helix) during extrusion, leading to a softer or more flexible texture. A high proportion of β-sheets and random coils contribute to a firmer and chewier or softer and tender texture, respectively. However, the β-sheet and random coil contents in our study did not directly correlate with the hardness or chewiness of extruded MPM. F1-55 and F5-55 exhibited the highest β-sheet contents (**Table 3**) but did not display the highest hardness or chewiness (**Table 2**). This suggests that other factors, such as the intermolecular bonds present within the protein structures, have a more significant influence on the textural properties of extruded MPM.

The helix-to-coil ratio identifies the conformational state and intermolecular interactions within the protein matrices. A higher helix-to-coil ratio indicates that the protein structure has retained a substantial amount of its native α-helical conformation (Lu et al., 2023). As the extrusion conditions for each extruded MPM were kept constant throughout, the degree of protein denaturation can be attributed to the protein combinations rather than the extrusion process. F1-55 exhibited the highest helix-to-coil ratio (**Table 3**), which was attributed to the high α-helices and low random coils of SPC (Mao et al., 2024).

3.6 Purine content

[Insert **Table 4**]

549 Beyond structure and texture, nutritional assessment is key for plant-based meat analogues.
550 While our previous study by Hua et al. (2023) delved into the amino acid composition of
551 extruded MPM, a holistic nutritional evaluation (i.e., purine content) remains imperative.
552 Purines, involved in vital processes, are metabolised to uric acid (Maiuolo et al., 2016); high
553 levels can cause hyperuricemia and gout (Kaneko et al., 2014; Vedder et al., 2019). While
554 meats are known purine sources, legumes also contribute (Vedder et al., 2019). Hence, this
555 study analysed purine content in selected extruded MPM, as shown in **Table 4**.
556
557 Among the analysed formulations, F4-55 exhibited the highest levels of adenine and guanine,
558 while F6-55 contained the most xanthine, hypoxanthine, and uric acid (**Table 4**). Despite the
559 predominant presence of RPI in F4, its low-purine nature as a whole grain contributed
560 minimally to the overall purine content. Conversely, the inclusion of MBPI in F4 may have
561 contributed to its elevated adenine and guanine levels. In F6, the presence of PPI and MBPI
562 could have influenced the higher concentrations of xanthine, hypoxanthine, and uric acid.
563 This aligns with the findings of Lontoc et al. (1993), who reported higher levels of guanine and
564 xanthine in legumes like green mung beans and peas. The total purine content in F1 (SPC and
565 WG) exceeded that of commercial meat alternatives analysed by Havlik et al. (2010). Although
566 the specific proportion of soy and wheat proteins in those meat alternatives was not specified,
567 the comparison highlights the potential variability in purine content among plant-based meat
568 analogues. Moreover, factors such as agricultural origins and extraction processing methods
569 may affect the composition and purine content of different plant proteins (Velázquez-
570 Martínez et al., 2022).
571

572 Therefore, findings from this study suggest that the specific ratios of these plant protein
573 combinations, rather than their mere presence, influence the overall purine content in the
574 extruded MPM. Our analysis revealed that the purine content of the extruded MPM was
575 lower than that reported for livestock and poultry (> 100 mg/ 100 g) (Hou et al., 2021). While
576 this level is generally considered safe for most individuals, it might be valuable to determine
577 the impact of the consumption of these extruded MPM on blood uric acid levels and its
578 associated risk for individuals with hyperuricemia in future *in-vivo* clinical studies.
579

580 ## 4. Conclusion

581 Extruded MPM designed to mimic the amino acid profile of chicken breast meat were
582 successfully developed in this study using various protein combinations. Extrusion at 55% and
583 60% MC resulted in MPM with distinct structural, textural, chemical, and nutritional
584 properties. Higher protein contents (31.82 - 41.61%) of MPM correlated with lower moisture
585 contents (51.18 - 53.93%), which were influenced by factors such as feed flow rates and
586 protein source-specific water-holding capacities. Our MPM had higher protein but lower
587 moisture than cooked chicken breast (28.94% and 71.46%, respectively). MPM exhibited
588 anisotropic structures with porosity ranging from 1.05% to 23.54%, influenced by protein
589 combinations and moisture content, which also affected hardness (105.34 - 281.26 N) and
590 chewiness (80.30 - 210.41 N), both of which were generally higher than those of cooked
591 chicken breast (40.53 - 55.01 N and 17.80 - 18.84 N). Secondary structure (β-sheet: 48.12 -
592 53.35%; random coil: 22.96 - 29.41%) showed no direct correlation with hardness or
593 chewiness. Purine content varied among protein combinations, with F4 and F6 exhibiting
594 elevated levels. Future research should focus on optimising MPM to further enhance their
595 textural and structural properties for a closer resemblance to cooked chicken breast.

Acknowledgement

This research was funded by the A*STAR BMRC (Biomedical Research Council) on SFS-2 IAF-PP Future Foods: Alternative Proteins: H20H8a0002 and was awarded to Jie Hong Chiang.

Declaration of interest

The authors declare that they have no conflict of interest.

Author contributions

Dayna Ong and Xin Yi Hua: Methodology, Formal analysis, Investigation, Writing – Original Draft, Writing – Review & Editing. **Alicia Theng, Bisma Mutiargo, and Hui Wen Lee**: Methodology, Formal analysis, Investigation, Writing – Review & Editing. **Raffael Osen**: Writing-Review & Editing. **Jie Hong Chiang**: Conceptualisation, Methodology, Visualisation, Writing-Review & Editing, Supervision, Project administration, Funding acquisition.

References

Brishti, F. H., Chay, S. Y., Muhammad, K., Ismail-Fitry, M. R., Zarei, M., & Saari, N. (2021). Texturized mung bean protein as a sustainable food source: Effects of extrusion on its physical, textural and protein quality. *Innovative Food Science & Emerging Technologies, 67*, 102591. doi:https://doi.org/10.1016/j.ifset.2020.102591

Chen, B., Yu, C., Liu, J., Yang, Y., Shen, X., Liu, S., & Tang, X. (2017). Physical properties and chemical forces of extruded corn starch fortified with soy protein isolate. *International*

618 *Journal of Food Science & Technology, 52*(12), 2604-2613.
619 doi:https://doi.org/10.1111/ijfs.13547
620 Chiang, J. H., Loveday, S. M., Hardacre, A. K., & Parker, M. E. (2019). Effects of soy protein to
621 wheat gluten ratio on the physicochemical properties of extruded meat analogues.
622 *Food Structure, 19*, 100102. doi:https://doi.org/10.1016/j.foostr.2018.11.002
623 Chiang, J. H., Tay, W., Ong, D. S. M., Liebl, D., Ng, C. P., & Henry, C. J. (2021). Physicochemical,
624 textural and structural characteristics of wheat gluten-soy protein composited meat
625 analogues prepared with the mechanical elongation method. *Food Structure, 28*,
626 100183. doi:https://doi.org/10.1016/j.foostr.2021.100183
627 De Angelis, D., Opaluwa, C., Pasqualone, A., Karbstein, H. P., & Summo, C. (2023). Rheological
628 properties of dry-fractionated mung bean protein and structural, textural, and
629 rheological evaluation of meat analogues produced by high-moisture extrusion
630 cooking. *Current Research in Food Science, 7*, 100552.
631 doi:https://doi.org/10.1016/j.crfs.2023.100552
632 Dekkers, B. L., Boom, R. M., & van der Goot, A. J. (2018). Structuring processes for meat
633 analogues. *Trends in Food Science & Technology, 81*, 25-36.
634 doi:https://doi.org/10.1016/j.tifs.2018.08.011
635 Dimina, L., Rémond, D., Huneau, J.-F., & Mariotti, F. (2022). Combining Plant Proteins to
636 Achieve Amino Acid Profiles Adapted to Various Nutritional Objectives—An
637 Exploratory Analysis Using Linear Programming. *Frontiers in Nutrition, 8*.
638 doi:10.3389/fnut.2021.809685
639 Ferawati, F., Zahari, I., Barman, M., Hefni, M., Ahlström, C., Witthöft, C., & Östbring, K. (2021).
640 High-Moisture Meat Analogues Produced from Yellow Pea and Faba Bean Protein
641 Isolates/Concentrate: Effect of Raw Material Composition and Extrusion Parameters

642 on Texture Properties. *Foods, 10*(4), 843. Retrieved from
643 https://www.mdpi.com/2304-8158/10/4/843
644 Ge, Y., Tang, Y., Guo, S., Liu, X., Zhu, Z., Zhang, L., . . . Duan, J.-a. (2016). Simultaneous
645 Quantitation of Free Amino Acids, Nucleosides and Nucleobases in Sipunculus nudus
646 by Ultra-High Performance Liquid Chromatography with Triple Quadrupole Mass
647 Spectrometry. *Molecules, 21*(4), 408. Retrieved from https://www.mdpi.com/1420-
648 3049/21/4/408
649 Godschalk-Broers, L., Sala, G., & Scholten, E. (2022). Meat Analogues: Relating Structure to
650 Texture and Sensory Perception. *Foods, 11*(15), 2227. Retrieved from
651 https://www.mdpi.com/2304-8158/11/15/2227
652 Gorissen, S. H. M., Crombag, J. J. R., Senden, J. M. G., Waterval, W. A. H., Bierau, J., Verdijk, L.
653 B., & van Loon, L. J. C. (2018). Protein content and amino acid composition of
654 commercially available plant-based protein isolates. *Amino Acids, 50*(12), 1685-1695.
655 doi:10.1007/s00726-018-2640-5
656 Guo, Z., Teng, F., Huang, Z., Lv, B., Lv, X., Babich, O., . . . Jiang, L. (2020). Effects of material
657 characteristics on the structural characteristics and flavor substances retention of
658 meat analogs. *Food Hydrocolloids, 105*, 105752.
659 doi:https://doi.org/10.1016/j.foodhyd.2020.105752
660 Havlik, J., Plachy, V., Fernandez, J., & Rada, V. (2010). Dietary purines in vegetarian meat
661 analogues. *Journal of the Science of Food and Agriculture, 90*(14), 2352-2357.
662 doi:https://doi.org/10.1002/jsfa.4089
663 Hou, C., Xiao, G., Amakye, W. K., Sun, J., Xu, Z., & Ren, J. (2021). Guidelines for purine
664 extraction and determination in foods. *Food Frontiers, 2*(4), 557-573.
665 doi:https://doi.org/10.1002/fft2.100

Hua, X. Y., Long, Y., Ong, D. S. M., Theng, A. H. P., Shi, J. K., Osen, R., . . . Chiang, J. H. (2023). Mathematical optimisation of extruded mixed plant protein-based meat analogues based on amino acid compositions. *Current Research in Food Science, 7*, 100648. doi:https://doi.org/10.1016/j.crfs.2023.100648

Jarpa-Parra, M. (2018). Lentil protein: a review of functional properties and food application. An overview of lentil protein functionality. *International Journal of Food Science & Technology, 53*(4), 892-903. doi:https://doi.org/10.1111/ijfs.13685

Jones, D. B. (1931). *Factors for converting percentages of nitrogen in foods and feeds into percentages of proteins* (Vol. 183): US Department of Agriculture Washington, DC.

Kaneko, K., Aoyagi, Y., Fukuuchi, T., Inazawa, K., & Yamaoka, N. (2014). Total Purine and Purine Base Content of Common Foodstuffs for Facilitating Nutritional Therapy for Gout and Hyperuricemia. *Biological and Pharmaceutical Bulletin, 37*(5), 709-721. doi:10.1248/bpb.b13-00967

Kołodziejczak, K., Onopiuk, A., Szpicer, A., & Poltorak, A. (2022). Meat Analogues in the Perspective of Recent Scientific Research: A Review. *Foods, 11*(1), 105. Retrieved from https://www.mdpi.com/2304-8158/11/1/105

Lee, J.-S., Choi, I., & Han, J. (2022a). Construction of rice protein-based meat analogues by extruding process: Effect of substitution of soy protein with rice protein on dynamic energy, appearance, physicochemical, and textural properties of meat analogues. *Food Research International, 161*, 111840. doi:https://doi.org/10.1016/j.foodres.2022.111840

Lee, J.-S., Kim, S., Jeong, Y. J., Choi, I., & Han, J. (2023). Impact of interactions between soy and pea proteins on quality characteristics of high-moisture meat analogues prepared

via extrusion cooking process. *Food Hydrocolloids, 139*, 108567. doi:https://doi.org/10.1016/j.foodhyd.2023.108567

Lee, J.-S., Oh, H., Choi, I., Yoon, C. S., & Han, J. (2022b). Physico-chemical characteristics of rice protein-based novel textured vegetable proteins as meat analogues produced by low-moisture extrusion cooking technology. *LWT, 157*, 113056. doi:https://doi.org/10.1016/j.lwt.2021.113056

Lendoiro, E., Cordeiro, C., Rodríguez-Calvo, M. S., Vieira, D. N., Suárez-Peñaranda, J. M., López-Rivadulla, M., & Muñoz-Barús, J. I. (2012). Applications of Tandem Mass Spectrometry (LC–MSMS) in estimating the post-mortem interval using the biochemistry of the vitreous humour. *Forensic Science International, 223*(1), 160-164. doi:https://doi.org/10.1016/j.forsciint.2012.08.022

Li, S., Zhang, H. Q., Jin, Z. T., & Hsieh, F.-h. (2005). Textural modification of soya bean/corn extrudates as affected by moisture content, screw speed and soya bean concentration. *International Journal of Food Science & Technology, 40*(7), 731-741. doi:https://doi.org/10.1111/j.1365-2621.2005.00993.x

Lin, S., Huff, H. E., & Hsieh, F. (2000). Texture and Chemical Characteristics of Soy Protein Meat Analog Extruded at High Moisture. *Journal of Food Science, 65*(2), 264-269. doi:https://doi.org/10.1111/j.1365-2621.2000.tb15991.x

Liu, K., & Hsieh, F.-H. (2008). Protein–Protein Interactions during High-Moisture Extrusion for Fibrous Meat Analogues and Comparison of Protein Solubility Methods Using Different Solvent Systems. *Journal of Agricultural and Food Chemistry, 56*(8), 2681-2687. doi:10.1021/jf073343q

711 Lontoc, A. V., Ladines, E. O., & Jalandoon, S. A. (1993). Purine content of some Philippine foods.
712 *Kimika*, 15-22. Retrieved from
713 http://inis.iaea.org/search/search.aspx?orig_q=RN:25024721
714 Lu, Z., Lee, P.-R., & Yang, H. (2023). Kappa-carrageenan improves the gelation and structures
715 of soy protein isolate through the formation of hydrogen bonding and electrostatic
716 interactions. *Food Hydrocolloids, 140*, 108585.
717 doi:https://doi.org/10.1016/j.foodhyd.2023.108585
718 Maiuolo, J., Oppedisano, F., Gratteri, S., Muscoli, C., & Mollace, V. (2016). Regulation of uric
719 acid metabolism and excretion. *International Journal of Cardiology, 213*, 8-14.
720 doi:https://doi.org/10.1016/j.ijcard.2015.08.109
721 Mao, B., Singh, J., Hodgkinson, S., Farouk, M., & Kaur, L. (2024). Conformational changes and
722 product quality of high-moisture extrudates produced from soy, rice, and pea proteins.
723 *Food Hydrocolloids, 147*, 109341. doi:https://doi.org/10.1016/j.foodhyd.2023.109341
724 Mariotti, F. (2017). 35 - Plant Protein, Animal Protein, and Protein Quality. In F. Mariotti (Ed.),
725 *Vegetarian and Plant-Based Diets in Health and Disease Prevention* (pp. 621-642):
726 Academic Press.
727 Mateen, A., & Singh, G. (2023). Evaluating the potential of millets as blend components with
728 soy protein isolate in a high moisture extrusion system for improved texture, structure,
729 and colour properties of meat analogues. *Food Research International, 173*, 113395.
730 doi:https://doi.org/10.1016/j.foodres.2023.113395
731 Monostori, P., Klinke, G., Hauke, J., Richter, S., Bierau, J., Garbade, S. F., . . . Okun, J. G. (2019).
732 Extended diagnosis of purine and pyrimidine disorders from urine: LC MS/MS assay
733 development and clinical validation. *PLOS ONE, 14*(2), e0212458.
734 doi:10.1371/journal.pone.0212458

735 Muguruma, Y., Tsutsui, H., Akatsu, H., & Inoue, K. (2020). Comprehensive quantification of
736 purine and pyrimidine metabolism in Alzheimer's disease postmortem cerebrospinal
737 fluid by LC–MS/MS with metal-free column. *Biomedical Chromatography, 34*(2),
738 e4722. doi:https://doi.org/10.1002/bmc.4722
739 Nieuwland, M., Heijnis, W., van der Goot, A.-J., & Hamoen, R. (2023). XRT for visualizing
740 microstructure of extruded meat replacers. *Current Research in Food Science, 6*,
741 100457. doi:https://doi.org/10.1016/j.crfs.2023.100457
742 Osen, R., Toelstede, S., Eisner, P., & Schweiggert-Weisz, U. (2015). Effect of high moisture
743 extrusion cooking on protein–protein interactions of pea (Pisum sativum L.) protein
744 isolates. *International Journal of Food Science & Technology, 50*(6), 1390-1396.
745 doi:https://doi.org/10.1111/ijfs.12783
746 Osen, R., Toelstede, S., Wild, F., Eisner, P., & Schweiggert-Weisz, U. (2014). High moisture
747 extrusion cooking of pea protein isolates: Raw material characteristics, extruder
748 responses, and texture properties. *Journal of Food Engineering, 127*, 67-74.
749 doi:https://doi.org/10.1016/j.jfoodeng.2013.11.023
750 Peng, J., Zhu, K.-X., Guo, X.-N., & Zhou, H.-M. (2021). The impact of phosphates on the fibrous
751 structure formation of textured wheat gluten. *Food Hydrocolloids, 119*, 106844.
752 doi:https://doi.org/10.1016/j.foodhyd.2021.106844
753 Peng, J., Zhu, K.-X., Guo, X.-N., & Zhou, H.-M. (2022). Egg white protein addition induces
754 protein aggregation and fibrous structure formation of textured wheat gluten. *Food*
755 *Chemistry, 371*, 131102. doi:https://doi.org/10.1016/j.foodchem.2021.131102
756 Ranasinghesagara, J., Hsieh, F.-H., & Yao, G. (2005). An Image Processing Method for
757 Quantifying Fiber Formation in Meat Analogs Under High Moisture Extrusion. *Journal*

758 *of Food Science, 70*(8), e450-e454. doi:https://doi.org/10.1111/j.1365-
759 2621.2005.tb11513.x
760 Schmid, E.-M., Farahnaky, A., Adhikari, B., & Torley, P. J. (2022). High moisture extrusion
761 cooking of meat analogs: A review of mechanisms of protein texturization.
762 *Comprehensive Reviews in Food Science and Food Safety, 21*(6), 4573-4609.
763 doi:https://doi.org/10.1111/1541-4337.13030
764 Schreuders, F. K. G., Dekkers, B. L., Bodnár, I., Erni, P., Boom, R. M., & van der Goot, A. J.
765 (2019). Comparing structuring potential of pea and soy protein with gluten for meat
766 analogue preparation. *Journal of Food Engineering, 261*, 32-39.
767 doi:https://doi.org/10.1016/j.jfoodeng.2019.04.022
768 Schreuders, F. K. G., Schlangen, M., Kyriakopoulou, K., Boom, R. M., & van der Goot, A. J.
769 (2021). Texture methods for evaluating meat and meat analogue structures: A review.
770 *Food Control, 127*, 108103. doi:https://doi.org/10.1016/j.foodcont.2021.108103
771 Scott, G., & Awika, J. M. (2023). Effect of protein–starch interactions on starch retrogradation
772 and implications for food product quality. *22*(3), 2081-2111.
773 doi:https://doi.org/10.1111/1541-4337.13141
774 Shand, P. J., Ya, H., Pietrasik, Z., & Wanasundara, P. K. J. P. D. (2007). Physicochemical and
775 textural properties of heat-induced pea protein isolate gels. *Food Chemistry, 102*(4),
776 1119-1130. doi:https://doi.org/10.1016/j.foodchem.2006.06.060
777 Snel, S. J. E., Otto, K., Schlangen, M., Beyrer, M., & van der Goot, A. J. (2024). Type of pectin
778 determines structuring potential of soy proteins into meat analogue applications.
779 *Food Hydrocolloids, 146*, 109262. doi:https://doi.org/10.1016/j.foodhyd.2023.109262

780 Taghian Dinani, S., Allaire, N., Boom, R., & van der Goot, A. J. (2023). Influence of processing
781 temperature on quality attributes of meat analogues fortified with l-cysteine. *Food*
782 *Hydrocolloids, 137*, 108422. doi:https://doi.org/10.1016/j.foodhyd.2022.108422
783 Tham, Z. W., Sampath, S., Chen, Y. F., Mutiargo, B., & Zhang, L. (2024). Non-contact defect
784 imaging of carbon fiber composites using laser excited acoustic shearography.
785 *Composites Science and Technology, 257*, 110796.
786 doi:https://doi.org/10.1016/j.compscitech.2024.110796
787 van der Sman, R. G. M., & van der Goot, A. J. (2023). Hypotheses concerning structuring of
788 extruded meat analogs. *Current Research in Food Science, 6*, 100510.
789 doi:https://doi.org/10.1016/j.crfs.2023.100510
790 van Vliet, S., Burd, N. A., & van Loon, L. J. C. (2015). The Skeletal Muscle Anabolic Response to
791 Plant- versus Animal-Based Protein Consumption1. *The Journal of Nutrition, 145*(9),
792 1981-1991. doi:https://doi.org/10.3945/jn.114.204305
793 Vedder, D., Walrabenstein, W., Heslinga, M., de Vries, R., Nurmohamed, M., van
794 Schaardenburg, D., & Gerritsen, M. (2019). Dietary Interventions for Gout and Effect
795 on Cardiovascular Risk Factors: A Systematic Review. *Nutrients, 11*(12), 2955.
796 Retrieved from https://www.mdpi.com/2072-6643/11/12/2955
797 Velázquez-Martínez, V., Valles-Rosales, D., Rodríguez-Uribe, L., Laguna-Camacho, J. R., López-
798 Calderón, H. D., & Delgado, E. (2022). Effect of Different Extraction Methods and
799 Geographical Origins on the Total Phenolic Yield, Composition, and Antimicrobial
800 Activity of Sugarcane Bagasse Extracts. *Frontiers in Nutrition, 9*.
801 doi:10.3389/fnut.2022.834557
802 Wang, C., Alavi, S., Li, Y., & Dogan, H. (2022a). Influence of chickpea flour and yellow pea
803 concentrate additive amount and in-barrel moisture content on the physiochemical

properties of extruded extrudates. *Journal of Food Processing and Preservation, 46*(2), e16233. doi:https://doi.org/10.1111/jfpp.16233

Wang, H., van den Berg, F. W. J., Zhang, W., Czaja, T. P., Zhang, L., Jespersen, B. M., & Lametsch, R. (2022b). Differences in physicochemical properties of high-moisture extrudates prepared from soy and pea protein isolates. *Food Hydrocolloids, 128*, 107540. doi:https://doi.org/10.1016/j.foodhyd.2022.107540

Wang, R., Zhang, L., Chi, Y., & Chi, Y. (2022c). Forces involved in freeze-induced egg yolk gelation: Effects of various bond dissociation reagents on gel properties and protein structure changes. *Food Chemistry, 371*, 131190. doi:https://doi.org/10.1016/j.foodchem.2021.131190

Wang, W., Shen, M., Liu, S., Jiang, L., Song, Q., & Xie, J. (2018). Gel properties and interactions of Mesona blumes polysaccharide-soy protein isolates mixed gel: The effect of salt addition. *Carbohydrate Polymers, 192*, 193-201. doi:https://doi.org/10.1016/j.carbpol.2018.03.064

Wang, Y., Zheng, Z., Zhang, C., Wu, C., Tan, C.-P., & Liu, Y. (2024). Comparative structural, digestion and absorption characterization of three common extruded plant proteins. *Food Research International, 177*, 113852. doi:https://doi.org/10.1016/j.foodres.2023.113852

Webb, D., Li, Y., & Alavi, S. (2023). Chemical and physicochemical features of common plant proteins and their extrudates for use in plant-based meat. *Trends in Food Science & Technology, 131*, 129-138. doi:https://doi.org/10.1016/j.tifs.2022.11.006

Wittek, P., Karbstein, H. P., & Emin, M. A. (2021). Blending Proteins in High Moisture Extrusion to Design Meat Analogues: Rheological Properties, Morphology Development and

827 Product Properties. *Foods, 10*(7), 1509. Retrieved from https://www.mdpi.com/2304-
828 8158/10/7/1509
829 Woolf, P. J., Fu, L. L., & Basu, A. (2011). vProtein: Identifying Optimal Amino Acid
830 Complements from Plant-Based Foods. *PLOS ONE, 6*(4), e18836.
831 doi:10.1371/journal.pone.0018836
832 Xia, S., Song, J., Ma, C., Hao, T., Hou, Y., Shen, S., . . . Jiang, X. (2023). Effects of moisture
833 content and processing temperature on the strength and orientation regulation of
834 fibrous structures in meat analogues. *Food Hydrocolloids, 145*, 109113.
835 doi:https://doi.org/10.1016/j.foodhyd.2023.109113
836 Zahari, I., Ferawati, F., Helstad, A., Ahlström, C., Östbring, K., Rayner, M., & Purhagen, J. K.
837 (2020). Development of High-Moisture Meat Analogues with Hemp and Soy Protein
838 Using Extrusion Cooking. *Foods, 9*(6), 772. Retrieved from
839 https://www.mdpi.com/2304-8158/9/6/772
840 Zhang, J., Liu, L., Jiang, Y., Faisal, S., & Wang, Q. (2020). A new insight into the high-moisture
841 extrusion process of peanut protein: From the aspect of the orders and amount of
842 energy input. *Journal of Food Engineering, 264*, 109668.
843 doi:https://doi.org/10.1016/j.jfoodeng.2019.07.015
844 Zhang, X., Zhao, Y., Zhang, T., Zhang, Y., Jiang, L., & Sui, X. (2022). High moisture extrusion of
845 soy protein and wheat gluten blend: An underlying mechanism for the formation of
846 fibrous structures. *LWT, 163*, 113561. doi:https://doi.org/10.1016/j.lwt.2022.113561
847 Zhao, H., Shen, C., Wu, Z., Zhang, Z., & Xu, C. (2020). Comparison of wheat, soybean, rice, and
848 pea protein properties for effective applications in food products. *Journal of Food*
849 *Biochemistry, 44*(4), e13157. doi:https://doi.org/10.1111/jfbc.13157

850 Zhao, Y., & Takhar, P. S. (2017). Micro X-ray computed tomography and image analysis of
851 frozen potatoes subjected to freeze-thaw cycles. *LWT - Food Science and Technology,*
852 *79*, 278-286. doi:https://doi.org/10.1016/j.lwt.2017.01.051

853

Tables

Table 1 Formulation and moisture content (%) of mixed protein matrices used for extrusion.

Sample	Moisture content (%)	Plant protein (%) [1]						
		SPC-1	SPC-2	WG	PPI	MBPI	CPC	RPI
F1	55	-	92.11	7.89	-	-	-	-
	60							
F2	55	-	44.92	7.32	-	-	47.76	-
	60							
F3	55	62.05	-	-	37.95	-	-	-
	60							
F4	55	34.70	-	-	-	13.58	-	51.72
	60							
F5	55	-	39.89	10.00	50.11	-	-	-
	60							
F6	55	-	-	10.00	66.81	23.19	-	-

[1] Abbreviation: SPC-1, soy protein concentrate (brand 1); SPC-2, soy protein concentrate (brand 2); WG, wheat gluten; PPI, pea protein isolate; MBPI, mung bean protein isolate; CPC, chickpea protein concentrate; RPI, rice protein isolate.

Table 2 Physicochemical (protein and moisture content), porosity, textural (hardness, chewiness and degree of texturisation) properties of extruded mixed protein matrices.

Sample	Protein (%)	Moisture (%)	Porosity (%)	Hardness (N)	Chewiness (N)	Degree of texturisation
F1-55	33.02 ± 0.06 ^{fg}	52.51 ± 1.08 ^{d}	3.63 ± 0.20 ^{e}	202.57 ± 21.68 ^{bc}	140.88 ± 15.73 ^{bc}	1.32 ± 0.10 ^{bcd}
F2-55	31.82 ± 0.25 ^{gh}	53.93 ± 1.73 ^{bcd}	15.95 ± 2.21 ^{b}	154.23 ± 6.13 ^{de}	111.92 ± 4.61 ^{de}	1.38 ± 0.12 ^{abcd}
F3-55	36.73 ± 0.72 ^{c}	51.18 ± 1.06 ^{d}	19.05 ± 0.78 ^{ab}	212.69 ± 18.69 ^{b}	153.14 ± 15.50 ^{b}	1.49 ± 0.19 ^{abc}
F4-55	38.78 ± 0.05 ^{b}	52.02 ± 0.76 ^{d}	16.97 ± 0.26 ^{b}	281.26 ± 17.52 ^{a}	210.41 ± 14.10 ^{a}	1.24 ± 0.23 ^{cd}
F5-55	34.90 ± 0.31 ^{d}	53.51 ± 0.68 ^{cd}	4.17 ± 0.13 ^{de}	175.20 ± 6.78 ^{cd}	127.82 ± 6.51 ^{cd}	1.72 ± 0.26 ^{a}
F6-55	41.61 ± 0.58 ^{a}	51.51 ± 0.62 ^{d}	19.29 ± 0.81 ^{ab}	159.19 ± 16.24 ^{de}	117.12 ± 12.50 ^{de}	1.07 ± 0.11 ^{d}
F1-60	26.39 ± 0.25 ^{i}	60.57 ± 2.23 ^{a}	2.41 ± 0.10 ^{e}	147.67 ± 12.75 ^{e}	102.42 ± 11.34 ^{e}	1.26 ± 0.06 ^{cd}
F2-60	30.56 ± 0.22 ^{h}	56.86 ± 0.74 ^{b}	9.55 ± 0.18 ^{c}	138.65 ± 10.50 ^{e}	96.43 ± 7.90 ^{ef}	1.67 ± 0.40 ^{ab}
F3-60	31.52 ± 0.56 ^{h}	56.11 ± 0.52 ^{bc}	9.29 ± 1.37 ^{cd}	157.15 ± 9.58 ^{de}	114.90 ± 3.79 ^{de}	1.11 ± 0.07 ^{d}
F4-60	34.56 ± 0.37 ^{de}	55.88 ± 1.13 ^{bc}	23.54 ± 5.13 ^{a}	179.54 ± 11.68 ^{cd}	129.16 ± 10.50 ^{cd}	1.27 ± 0.09 ^{cd}
F5-60	33.91 ± 0.45 ^{ef}	54.20 ± 0.27 ^{bcd}	1.05 ± 0.07 ^{e}	105.34 ± 15.52 ^{f}	80.30 ± 11.73 ^{f}	1.43 ± 0.15 ^{abcd}
F6-60	NA	NA	NA	NA	NA	NA

p-value	0.000	0.000	0.000	0.000	0.000	0.000
F-value	219.20	18.66	280.66	63.76	58.32	7.20

[1] Data are presented as the mean and standard deviation of three replicates.

Values bearing different lowercase letters under the same column were significantly different ($p \leq 0.05$) according to Tukey's post hoc test.

Table 3 Relative proportion of the secondary structures of the extruded mixed protein matrices (MPM; F1 to F6) at the moisture content of 55% w/w.

Sample	Relative content (%) [1]				
	β-sheets	Random coil	α-helix	β-turns	Helix/coil
F1-55	53.00 ± 3.63^{ab}	22.96 ± 2.68^{c}	18.09 ± 1.80^{a}	5.95 ± 0.31^{c}	0.79 ± 0.12^{a}
F2-55	48.12 ± 1.01^{c}	29.37 ± 0.61^{a}	15.19 ± 0.45^{b}	7.32 ± 0.13a^{b}	0.52 ± 0.01^{b}
F3-55	48.64 ± 0.77^{abc}	29.01 ± 0.48^{ab}	14.77 ± 0.09^{b}	7.59 ± 0.22^{ab}	0.51 ± 0.01^{b}
F4-55	48.67 ± 0.47^{abc}	28.69 ± 0.36^{ab}	16.16 ± 0.72^{ab}	6.47 ± 0.82^{bc}	0.56 ± 0.03^{b}
F5-55	53.35 ± 1.62^{a}	25.70 ± 0.99^{bc}	14.03 ± 1.23^{b}	6.92 ± 0.73^{bc}	0.55 ± 0.03^{b}
F6-55	48.51 ± 0.75^{bc}	29.41 ± 0.43^{a}	13.63 ± 0.49^{b}	8.45 ± 0.21^{a}	0.46 ± 0.01^{b}
p-value	0.006	0.000	0.001	0.001	0.000
F-value	5.84	13.77	8.28	9.81	14.95

[1] Data are presented as the mean and standard deviation of three replicates.

Values bearing different lowercase letters under the same column were significantly different ($p \leq 0.05$) according to Tukey's post hoc test.

Table 4 Concentration of purines (i.e., adenine, guanine, xanthine, uric acid, and hypoxanthine) present in the selected extruded mixed protein matrices (MPM; F1 to F6)

Sample	Concentration (mg/ 100 g) [1]				
	Adenine	Guanine	Xanthine	Hypoxanthine	Uric acid
F1-55	66.28 ± 2.43 [b]	74.66 ± 1.30 [b]	1.29 ± 0.03 [b]	0.68 ± 0.10 [a]	0.03 ± 0.01 [a]
F2-55	45.35 ± 3.33 [a]	53.91 ± 4.03 [a]	1.01 ± 0.03 [a]	0.65 ± 0.06 [a]	0.03 ± 0.01 [a]
F3-55	71.82 ± 3.29 [bc]	79.62 ± 1.41 [bc]	1.65 ± 0.02 [c]	0.81 ± 0.12 [a]	0.07 ± 0.02 [a]
F4-55	80.31 ± 7.65 [c]	101.47 ± 8.01 [d]	2.78 ± 0.22 [e]	1.64 ± 0.16 [b]	0.09 ± 0.02 [a]
F5-55	69.58 ± 1.56 [bc]	80.17 ± 1.79 [bc]	1.98 ± 0.06 [d]	0.86 ± 0.06 [a]	0.12 ± 0.03 [ab]
F6-55	76.52 ± 1.96 [bc]	89.57 ± 2.47 [c]	3.55 ± 0.04 [f]	2.10 ± 0.38 [b]	0.22 ± 0.07 [b]
p-value	0.000	0.000	0.000	0.000	0.000
F-value	29.37	48.45	298.51	32.77	10.53

[1] Data are presented as the mean and standard deviation of three replicates.

Values bearing different lowercase letters under the same column were significantly different (p≤0.05) according to Tukey's post hoc test.

Figures

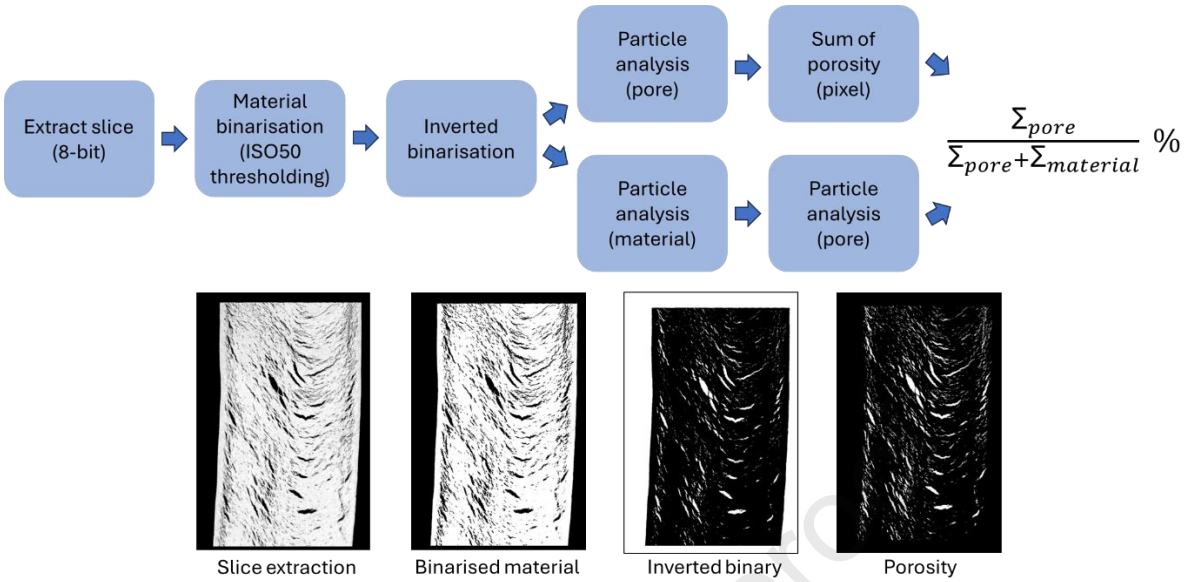

Figure 1 Methodology for image analysis for porosity.

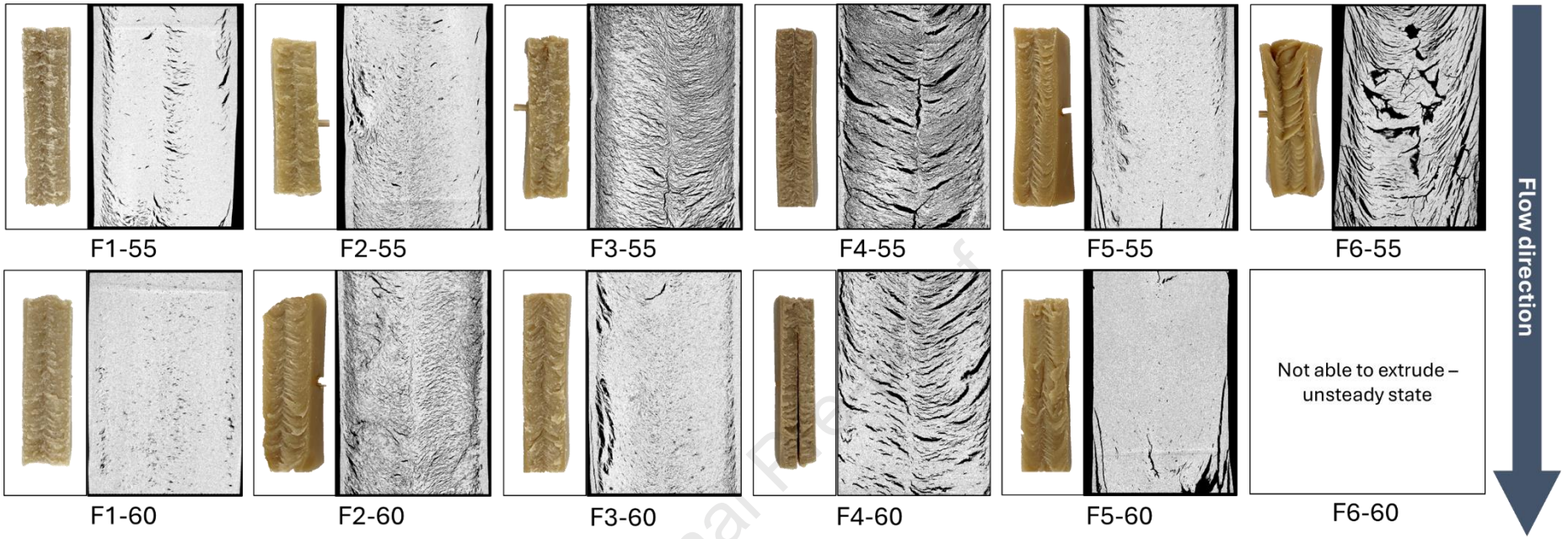

Figure 2 Visual appearance and X-ray computed tomography (XCT) images of the longitudinal cross-section of the extruded mixed protein matrices (MPM; F1 to F6) at 55% and 60% w/w moisture content. A shallow incision parallel to the flow direction was made to allow the breaking of the extrudates.

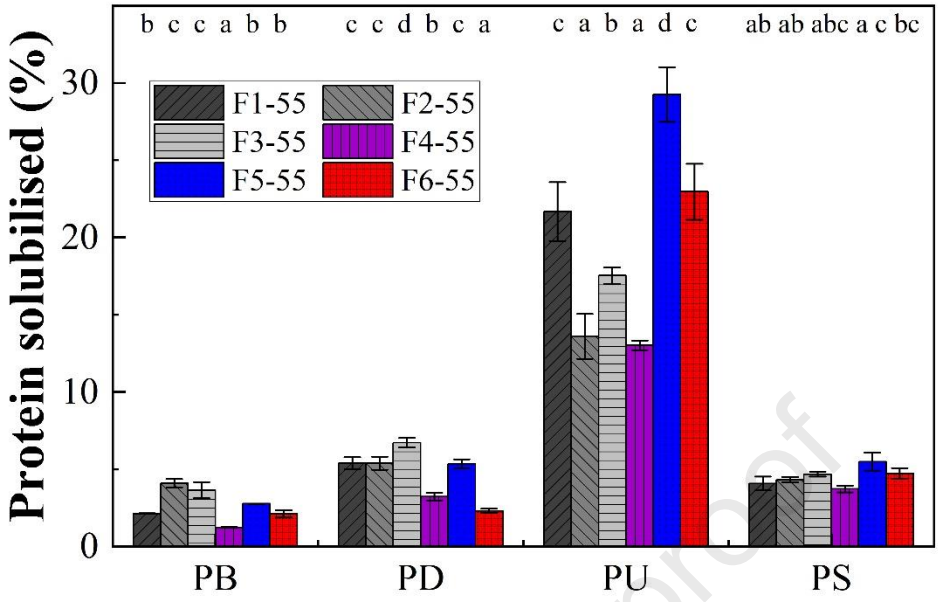

Figure 3 The amount of solubilised protein from selected extruded mixed protein matrices (MPM; F1 to F6 at the moisture content of 55% w/w), induced by different extracting solvents P (native state), PD (disulphide bonds), PU (hydrogen bonds), and PS (hydrophobic interactions). Data are presented as the mean and standard deviation of three replicates. Overall one-way ANOVA was found to be significant ($p \leq 0.05$). Values bearing different lowercase letters under the same extraction solutions (e.g., PB, PD, PU, or PS) were significantly different according to Tukey's post hoc test.

Highlights

- Six mixed protein matrices (MPM) combinations extruded at 55% and 60% moisture.
- X-ray computed tomography assessed the MPM's macrostructure and porosity.
- Hydrogen bonds and β-sheets dominated the MPM’s structure.
- The purine content of MPM was lower than that of commercial vegetarian products.

Declaration of interests

☒ The authors declare that they have no known competing financial interests or personal relationships that could have appeared to influence the work reported in this paper.

☐The authors declare the following financial interests/personal relationships which may be considered as potential competing interests: